

High-entropy ceramics: propelling applications through disorder

Cormac Toher,¹ Corey Oses,¹ Marco Esters,¹ David Hicks,¹ George N. Kotsonis,² Christina M. Rost,³ Donald W. Brenner,⁴ Jon-Paul Maria,² and Stefano Curtarolo^{1,*}

¹*Dept. Mechanical Engineering and Materials Science and Center for Autonomous Materials Design, Duke University, Durham, NC 27708, USA*

²*Dept. Materials Science and Engineering, The Pennsylvania State University, University Park, PA 16802, USA*

³*Dept. Physics and Astronomy, James Madison University, Harrisonburg, VA 22807, USA*

⁴*Dept. Materials Science and Engineering, North Carolina State University, Raleigh, NC 27695, USA*

(Dated: November 24, 2021)

Disorder enhances desired properties, as well as creating new avenues for synthesizing materials. For instance, hardness and yield stress are improved by solid-solution strengthening, a result of distortions and atomic size mismatches. Thermo-chemical stability is increased by the preference of chemically disordered mixtures for high-symmetry super-lattices. Vibrational thermal conductivity is decreased by force-constant disorder without sacrificing mechanical strength and stiffness. Thus, high-entropy ceramics propel a wide range of applications: from wear resistant coatings and thermal and environmental barriers to catalysts, batteries, thermoelectrics and nuclear energy management. Here, we discuss recent progress of the field, with a particular emphasis on disorder-enhanced properties and applications.

INTRODUCTION

Entropy is expected to dominate the formation of single-phase multicomponent ceramics [1], opening up new synthesis routes and facilitating property optimization without the need for toxic or expensive elements. High-entropy ceramics [2] typically consist of a disordered multi-cation sublattice and an ordered single-anion sublattice [3], with multi-anion ceramics now also being developed [4–6]. The earliest work on high-entropy ceramics involved thin films synthesized by sputtering high-entropy alloys in a N₂ or O₂ atmosphere [7–9]. The original attempts typically resulted in amorphous or multi-phase films due to the presence of non-nitride forming metals such as Cu [7, 8]; while the first single-phase high-entropy ceramic thin film reported was (AlCrTaTiZr)N, displaying an fcc lattice based on the rocksalt structure [9]. In 2015, (MgCoNiCuZn)O became the first bulk single-phase high-entropy ceramic to be synthesized — it also displayed a rocksalt-type fcc lattice [3], and was demonstrated to be entropy-stabilized: when annealed at high temperatures, the non-cubic CuO and ZnO secondary phases merged with the rocksalt phase [3]. High-entropy ceramics have now expanded to include carbides [10], borides [11], silicides [12], niobates [13, 14], zirconates [15, 16], as well as multi-anion boro-carbides [4] and carbo-nitrides [5, 6].

In addition to contributing to synthesizability, disorder directly alters and improves the properties of materials such as high-entropy ceramics [2]. Solid-solution strengthening combined with reduced grain growth enhances mechanical properties including strength, hardness and toughness [10, 17–19] — vital for structural applications and wear resistant coatings [20]. The strong thermodynamic preference for high-symmetry lattices increases the thermo-chemical stability, suppressing struc-

tural defect formation and phase transitions — crucial for thin-film diffusion barriers in nanoelectronics [21] and for improving cycling ability in battery materials [22, 23] — while entropic stabilization of unusual oxidation states opens up catalyst design rules [24]. Interatomic force constant and mass disorder reduce lattice thermal conductivity, often reaching the amorphous limit [25] — useful for increasing the efficiency of thermoelectric devices [26–28]. The combination of low thermal conductivity, mechanical strength and corrosion resistance make high-entropy ceramics particularly suitable as thermal and environmental barriers (*e.g.*, for hypersonics) [13–16]. In magnetic systems, disorder introduces localization, reducing the orbital overlap and increasing the importance of double and superexchange [29], while disrupting long-range order promotes the formation of relaxor ferroelectrics [30–32].

SYNTHESIS AND MODELING TECHNIQUES

Synthesis approaches. Synthesis techniques for high-entropy ceramics include sputtering [7–9]; pulsed laser deposition [33]; (reactive) spark plasma sintering [10, 34]; boro-, carbo- and boro-carbothermal synthesis [35]; sol-gel synthesis [24]; and solution combustion synthesis [36]. One current research direction is developing techniques to avoid grain-coarsening to enhance mechanical properties, such as new spark-plasma sintering protocols with lower temperatures or shorter annealing times [37], or carbothermal synthesis using finely ground metal or metal oxide precursors [35, 38]. Growth kinetics (*e.g.*, substrate temperature for pulsed laser deposition) and epitaxial strain can be used to engineer electrical and magnetic properties [33]. Rapid high-temperature Joule heating was used to synthesize a Pd-containing denary nanoparticle catalyst for methane combustion [39], where short, high-temperature heat treatments overcame the kinetic barriers for mixing multiple elements while avoiding agglomeration and collapse of pore structure.

* stefano@duke.edu

Computational modeling. First-principles modeling of disordered materials often uses special quasi-random structures (SQS) [40], in which the lattice is decorated so as to maximize the similarity of the radial correlation functions to that of the completely disordered material, in combination with the ideal approximation for the configurational entropy. SQS models the fully disordered, infinite-temperature limit: useful for understanding how high levels of disorder can affect properties, but neglecting the effect of short- and long-range ordering at finite temperatures.

The AFLOW partial occupation module (AFLOW-POCC) enables the modeling of disorder as a function of temperature [41]. The disordered material is represented by an ensemble of small ordered cells, generated by enumerating all possible decorations of the parent structure that produce the target compositions up to a cell-size cut-off. A descriptor, the entropy forming ability (EFA), was formulated based on the energy distribution obtained from first-principles calculations of these configurations [10]. A narrow distribution implies that it is easy to introduce new configurations and disorder, while a broad distribution indicates a thermodynamic preference for certain ordered states. The EFA descriptor has guided the synthesis of high-entropy carbides, successfully predicting whether compositions would form a single-phase or undergo phase separation [10]. Cr-containing compositions forming a single phase were also identified with machine-learning models trained on EFA data [42].

The properties of high-entropy ceramics have also been modeled computationally [10, 43, 44]. AFLOW-POCC was used to calculate the thermodynamically weighted average of the elastic moduli of the different configurations to predict the mechanical properties of disordered carbides [10]. The temperature-dependent elastic properties of (HfTaTiWZr)C and (MoNbTaVW)C and their component binary carbides were investigated using *ab initio* molecular dynamics [43]. Molecular dynamics simulations with deep-learning potentials were used to predict the thermal and elastic properties of (HfNbTaTiZr)B₂ as a function of temperature [44].

DISORDER-ENHANCED PROPERTIES

Mechanical properties. The mechanical properties of high-entropy ceramics are enhanced by a combination of grain refinement and solid-solution strengthening — lattice distortions due to differing atomic radii and Jahn-Teller effects [47, 48] create barriers that disrupt the propagation of dislocations, hindering plastic deformation and increasing hardness and yield strength. The reduction in grain coarsening has been attributed to increased crystalline energy due to lattice distortions, which reduces the free energy gained by shrinking the grain surface area [49, 50], as well as to slow diffusion [50]. Finer grains lead to improved toughness, and to Hall-Petch strengthening due to the nanograin microstructure

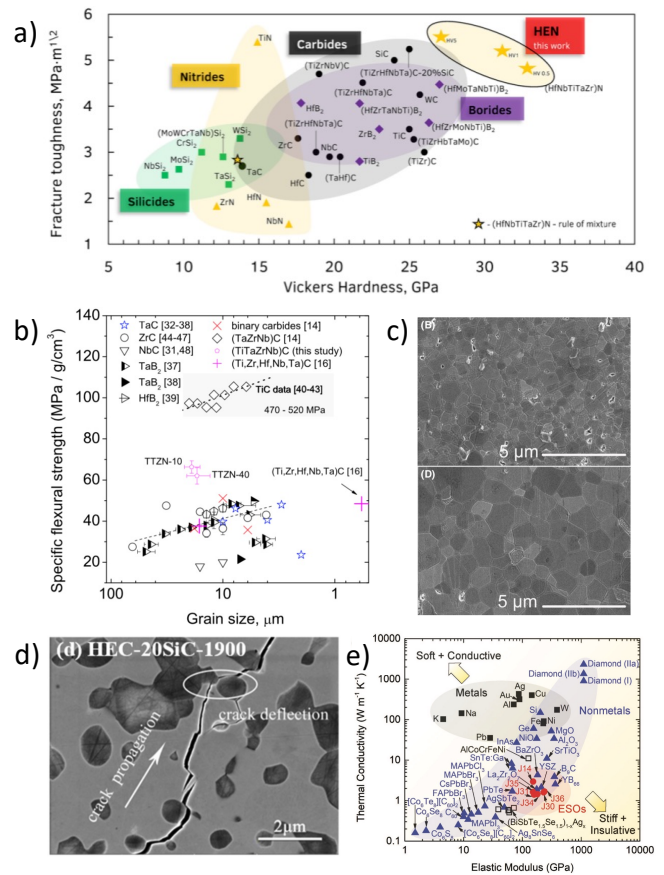


FIG. 1. Thermal and mechanical properties. **a)** Disorder simultaneously enhances hardness and fracture toughness of high-entropy nitrides (panel adapted from Ref. 19). **b)** Flexural strength as a function of grain size (panel adapted from Ref. 45). **c)** Microstructures of (HfNbTaTiZr)C annealed at 1800°C (top) and 1900°C (bottom), showing the increase in grain size with temperature (panel adapted from Ref. 38). **d)** Crack deflection by SiC phase (panel adapted from Ref. 46). **e)** Thermal conductivity *versus* elastic modulus: disorder lowers thermal conductivity while maintaining stiffness (panel adapted from Ref. 25).

impeding the motion of dislocations.

Bulk (HfNbTaTiZr)C, prepared by spark-plasma sintering, shows a hardness 50% higher than what would be expected from the rule-of-mixtures of the binary carbides [10, 17, 51], while carbo-nitride versions of this composition are slightly harder than the carbides [5, 6], and an 8-cation carbide is even harder [52]. High-entropy nitrides show even greater improvements, doubling both hardness and fracture toughness compared to their components (Figure 1a) [19]. Thin films deposited using magnetron sputtering had even higher hardness [53–55], likely due to internal stresses induced by ion bombardment [53–55]: the highest reported hardness was 70 GPa for a (HfNbTaTiV)N film [56]. The highest fracture toughness values of 8.4 MPa m^{1/2} were reported for (MoNbTaTiVW)C(N) [57], whereas the highest flexural strengths

The magnetic and electrical properties of high-entropy ceramics can be tuned by altering their composition [69, 70] or synthesis conditions [33, 70], or by applying strain [29, 67]. (MgCoNiCuZn)O films grown at low temperature exhibit enhanced Co^{3+} concentrations that result in a compressed lattice parameter, reduced optical band gap, increased electrical conductivity, and more diluted magnetic lattice [33, 70]. Tensile strain generates magnetic anisotropy by increasing the out-of-plane magnetic hardness (Figure 2a) [29], apparently due to the modification of the superexchange coupling between the transition metal atoms. Increasing the Cu content of (MgCoNiCuZn)O creates structural disorder since Cu^{2+} ions tend to undergo a tetragonal distortion from the octahedral coordination (Jahn-Teller effect [48]), leading to increased spin frustration and a reduction in the driving force for a preferred magnetization axis [69]. Increasing the non-magnetic Co^{3+} concentration in (MgCoNiCuZn)O results in more uncompensated spins when interfaced with a ferromagnet, leading to enhanced magnetic exchange bias [33].

Relaxor ferroelectrics have much smaller permanent electric dipole domains than conventional ferroelectrics, forming “polar nano-regions” on the nanoscale instead of the microscale. They take less energy to align, giving them very high specific capacitance and making them useful for energy storage. They also have high dielectric permittivity, high piezoelectric coefficient and giant field induced strain: important for applications in dielectric capacitors, piezoelectric sensors and actuators. In high-entropy ceramics such as perovskite-structure (NaBiBaSrCa)TiO₃ and (BiNaKBaCa)TiO₃, or Aurivillius phase (CaSrBaPb)Bi₂Nb₂O₉ and (Ca_{0.2}Sr_{0.2}Ba_{0.2}Pb_{0.2}Nd_{0.1}Na_{0.1})Bi₂Nb₂O₉ (space group $A2_1am$, #36), differences in the valence and ion size disrupt long-range ferroelectric ordering and result in the formation of several different types of electric dipoles. This promotes the formation of polar nano-regions, reducing the saturation polarization, remanent polarization and coercive field [30–32], and increasing the piezoelectric coefficients [32]. (NaBiBaSrCa)TiO₃ also displayed an electrocaloric effect: the application of an electric field changes the dipole arrangement from disordered to ordered, resulting in an entropy-change that can be exploited for refrigeration [30].

Corrosion resistance. The high melting temperatures of carbides and borides offer great potential for applications in extreme environments such as combustion chambers, where resistance against corrosion is critical. Oxidation behavior has been extensively studied in (HfNbTaTiZr)C [71–75]. Kinetic investigations showed that oxidation follows a parabolic rate law between 1073 and 1773 K, indicating a diffusion-controlled process [71–73]. The rate constant increases until 1273 K while the passivating layer is highly porous, then decreases with increasing temperature as more complex quaternary and quinary oxides form and the passivating layer densifies [71, 72]. The oxide layer is heterogeneous: group IV ox-

ides primarily form near the surface (due to the readily oxidized corresponding carbides), while group V oxides form near the interface with the ceramic [74, 75] — similar results were found in the diboride analog [74, 75]. Experiments using water vapor showed a denser protective layer, which increased corrosion resistance by preventing inward diffusion of H₂O [73]. The same study found improved corrosion resistance compared to ZrC — attributed to sluggish diffusion in the high-entropy material due to lattice distortions, suppressing outward diffusion of the cations. This was supported by decreased oxidation rates in (HfNbTaTiZr)C compared to (TiNbTaZr)C and (NbTiZr)C.

A separate study in air found improved oxidation resistance in (HfNbTaZr)C compared to the five-metal carbide [76, 77]. The four-metal carbide also showed improved performance compared to the binary carbide reactants, and the oxide layer was more structurally stable than in (HfTa)C, even though (HfTa)C had a lower oxidation onset temperature [76]. Mechanistic studies confirmed that outward diffusion of TiO is the rate-determining step in the oxidation of (HfNbTaTiZr)C and thus key to increased corrosion resistance of (HfNbTaZr)C [78]. Performance was further improved by doping with SiC as it forms a dense oxide that prevents inwards diffusion of oxygen. Additionally, SiO is an effective diffusion barrier for Ta and Nb oxides, preventing outward diffusion of these metals [77, 78]. (HfNbTaZr)C with 20 vol-% SiC showed enhanced oxidation resistance compared to the ultra-high temperature ceramic ZrB₂-SiC [77]. Composition and porosity of the passivating oxide layer are therefore crucial to the stability of high-entropy ceramics at high temperatures under oxidizing conditions. The ability to combine many elements to tailor chemical properties makes high-entropy carbides and borides strong candidates for applications in extreme heat conditions.

HIGH-ENTROPY CERAMIC APPLICATIONS

Batteries. The entropy-driven preference for high-symmetry lattices gives materials such as (MgCoNiCuZn)O high thermo-chemical stability, suppressing structural deformation and defect formation, giving them the potential to maintain performance under charge cycling (Figure 2b) [22, 79]. This led to investigations of the suitability of high-entropy ceramics for use as anodes, cathodes and solid-state electrolytes in Li-ion batteries [22, 23]. Shortly after its initial synthesis, room temperature superionic conductivity was reported for Li-doped (MgCoNiCuZn)O [80], significantly exceeding that of the currently-used lithium phosphorous oxy-nitride solid-state electrolyte.

High-entropy oxides based on (MgCoNiCuZn)O are also promising as anodes, with high specific capacities and robust responses to charge cycling. Initial capacities of 980 mAh g⁻¹ [22] to 1585 mAh g⁻¹

[79] have been reported, with a reversible capacity of 920 mAh g⁻¹ at 100 mA g⁻¹ after 300 cycles [79]. (MgCuNiZn)_{0.65}Li_{0.35}O had an even higher initial discharge capacity of 1930 mAh g⁻¹ [81]. These values compare very favorably with the current standard graphite anodes, which have a capacity of ~360 mAh g⁻¹ [23].

Cation-disordered rocksalt-type oxyfluorides were investigated for use as Li-ion cathodes [82], delivering specific energies of up to 307 mAh g⁻¹. High-entropy oxides based on the layered delafossite α -NaFeO₂ structures were also examined, but their specific capacities were low compared to state-of-the-art cathode materials [83].

X-ray absorption spectroscopy was used to investigate the lithiation mechanisms in (MgCoNiCuZn)O [84, 85]. Cu(II) was observed to reduce first to Cu(I) and then to metallic Cu, followed by reduction of Ni and Co to the metallic state. The high-entropy oxide structure appeared to collapse for charges greater than 400 mAh g⁻¹, and at 800 mAh g⁻¹, a significant portion of Zn metal was present [85]. Removing Zn or Mg from (MgCoNiCuZn)O resulted in significantly worse cycling performance, indicating that these cations are important for maintaining the rocksalt structure.

Catalysts. High-entropy catalysts, particularly oxides, demonstrate several advantages over ordered counterparts: compositional freedom translating to substantial electronic structure and coordination environment tunability [39, 86], better performance than fewer-component variants [39, 86], and excellent stability and durability [24, 86–88]. High entropy enables the design of new catalysts that combine and even enhance beneficial features of their components. In FeNiCoCrMn-glycerate, Fe-, Ni-, Co-, and Mn-based materials are known to be highly active oxygen evolution reaction electrocatalysts [86], while Cr induces strain in the structure that weakens active site chemisorption. The layered glycerate structure allows rapid transport of the reactants to the material and provides additional catalytic active sites. High entropy can also stabilize exotic active sites: Cu in high-entropy rocksalt phases can cycle between redox states Cu(II) and Cu(I) as it is treated with CO and O₂ at temperatures from 130°C to ~250°C [24], whereas CuO is irreversibly reduced to Cu(I) under the same conditions.

Poly-cation oxides like (FeMgCoNi)O_{1.2} have shown great potential for hydrogen production through two-step thermochemical water splitting [87, 89]. Improvements have been reported by integrating microwave-absorbing SiC foam and performing the reaction under short-term, low-energy microwave irradiation: **i.** the thermal reduction process was expedited to 4 minutes versus the usual 30 minutes or greater, **ii.** high H₂ generation rates, and **iii.** power consumption that is 3% that of conventional heat treatments. Microwave irradiation significantly increases the oxygen vacancies in the structure and can also generate plasma that enhances hydrogen production, but at the cost of accelerated degradation of the material.

High-entropy structures were also shown to be a cat-

alytic booster for aerobic oxidative desulfurization of diesel [90]. Carbon and oxygen co-doped hexagonal boron nitride catalysts with the highest density of grain boundaries demonstrated the shortest induction period, achieving complete sulfur conversion in six hours.

Thermoelectrics. Thermoelectric materials generate a voltage when subjected to a thermal gradient, and are used for energy generation and refrigeration. They are evaluated by the “figure of merit”: $zT = \sigma S^2/\kappa$, where σ is the electrical conductivity, S is the Seebeck coefficient and κ is the thermal conductivity — the reduced lattice thermal conductivity in disordered materials leads to increased zT . The thermal conductivity of perovskite-structure (BaCaLaPbSr)TiO₃ was ~5 times lower than that of SrTiO₃ [26], with a maximum zT over 0.2. The high-entropy chalcogenide Pb_{0.89}Sb_{0.012}Sn_{0.1}Se_{0.5}Te_{0.25}S_{0.25} had an ultralow thermal conductivity of 0.3 W m⁻¹ K⁻¹ [27] with zT of 1.8 compared to 0.8 for Pb_{0.99}Sb_{0.012}Se (Figure 2c). Adding Sn enabled the stabilization of the Pb(SeTeS) system due to increased configurational entropy. Pb_{0.975-x}Cd_xNa_{0.025}Se_{0.5}S_{0.25}Te_{0.25}, where $x \leq 0.05$, had a conversion efficiency at $\Delta T = 507$ K of 12% (among the highest reported values) with a power output of 2.7 W [28].

Thermal and environmental barriers. The simultaneous suppression of the thermal conductivity [25] and enhancement of the mechanical properties [10, 51] in high-entropy materials makes them highly attractive for thermal and environmental protection applications, with recent work focusing on niobates [13, 14] and zirconates [15, 16]. Pyrochlore-structure (LaNdSmEuGd)₂Zr₂O₇ could withstand up to 5 times as much thermal cycling as La₂Zr₂O₇ [15]. Rare earth niobates had ultra-low thermal conductivities of < 1 W m⁻¹ K⁻¹ [13] and hardnesses up to 13.9 GPa [14].

Nuclear energy applications. Their thermochemical stability and mechanical behavior make high-entropy materials promising for nuclear energy applications ranging from **i.** structural components in fission and fusion reactors, which need resistance to neutron irradiation damage, corrosive coolants, thermal and irradiation creep, helium embrittlement, etc. [91]; to **ii.** immobilizing matrices for high-level waste, which require excellent radiation tolerance and aqueous durability [68]. Radiation-induced defect clusters and dislocation loops in (NbTaTiZr)C remained small — likely due to the lattice distortion slowing their growth — and no void formation or radiation-induced segregation near grain boundaries were observed [91]. For pyrochlore-structure (Eu_{1-x}Gd_x)₂(TiZrHfNbCe)₂O₇, the normalized leaching rates for simulated radionuclides Ce (surrogate for Pu) and Gd were two orders of magnitude lower than that for Gd₂Zr₂O₇ (Figure 2d). Electrical conductivity was much lower in the high-entropy material, indicating significantly fewer oxygen vacancies — leading to slower cation diffusion and higher chemical stability — while lattice distortion also leads to a high lattice potential en-

ergy, reducing cation mobility.

CONCLUSIONS

Disorder is propelling the development of new ceramic materials. Configurational entropy provides new thermodynamic pathways to stabilize multi-component materials. Disorder directly enhances properties, facilitating the design of materials with features that are traditionally considered mutually exclusive, such as high stiffness and low thermal conductivity, or improved hardness and fracture toughness. High-entropy ceramics will continue

to impact fields as diverse as batteries, catalysts, thermoelectrics, magnets, ferroelectrics, nuclear energy, and structural materials, for the foreseeable future.

Acknowledgments. The authors thank Xiomara Campilongo, Eva Zurek, William Fahrenholtz, Douglas Wolfe and Darrell Schlom for valuable discussions. Research sponsored by DOD-ONR (N00014-15-1-2863, N00014-21-1-2515) and NSF (DMR-1921909, DGE-2022040).

Author contributions. The authors contributed equally to the article.

Competing interests. The authors declare no competing interests.

-
- [1] C. Toher, C. Oses, D. Hicks, and S. Curtarolo, *npj Comput. Mater.* **5**, 69 (2019).
- [2] C. Oses, C. Toher, and S. Curtarolo, *Nat. Rev. Mater.* **5**, 295–309 (2020).
- [3] C. M. Rost, E. Sachet, T. Borman, A. Moballeggh, E. C. Dickey, D. Hou, J. L. Jones, S. Curtarolo, and J.-P. Maria, *Nat. Commun.* **6**, 8485 (2015).
- [4] M. Qin, J. Gild, C. Hu, H. Wang, M. S. B. Hoque, J. L. Braun, T. J. Harrington, P. E. Hopkins, K. S. Vecchio, and J. Luo, *J. Eur. Ceram. Soc.* **40**, 5037–5050 (2020).
- [5] O. F. Dippo, N. Mesgarzadeh, T. J. Harrington, G. D. Schrader, and K. S. Vecchio, *Sci. Rep.* **10**, 21288 (2020).
- [6] T. Wen, B. Ye, M. C. Nguyen, M. Ma, and Y. Chu, *J. Am. Ceram. Soc.* **103**, 6475–6489 (2020).
- [7] T.-K. Chen, T. T. Shun, J.-W. Yeh, and M. S. Wong, *Surf. Coat. Technol.* **188–189**, 193–200 (2004).
- [8] T.-K. Chen, M.-S. Wong, T.-T. Shun, and J.-W. Yeh, *Surf. Coat. Technol.* **200**, 1361–1365 (2005).
- [9] C.-H. Lai, S.-J. Lin, J.-W. Yeh, and S.-Y. Chang, *Surf. Coat. Technol.* **201**, 3275–3280 (2006).
- [10] P. Sarker, T. Harrington, C. Toher, C. Oses, M. Samiee, J.-P. Maria, D. W. Brenner, K. S. Vecchio, and S. Curtarolo, *Nat. Commun.* **9**, 4980 (2018).
- [11] J. Gild, Y. Zhang, T. Harrington, S. Jiang, T. Hu, M. C. Quinn, W. M. Mellor, N. Zhou, K. Vecchio, and J. Luo, *Sci. Rep.* **6**, 37946 (2016).
- [12] J. Gild, J. Braun, K. Kaufmann, E. Marin, T. J. Harrington, P. E. Hopkins, K. S. Vecchio, and J. Luo, *J. Materiomics* **5**, 337–343 (2019).
- [13] J. Zhu, X. Meng, J. Xu, P. Zhang, Z. Lou, M. J. Reece, and F. Gao, *J. Eur. Ceram. Soc.* **41**, 1052–1057 (2021).
- [14] L. Chen, Y. Wang, M. Hu, L. Zhang, J. Wang, Z. Zhang, X. Liang, J. Guo, and J. Feng, *Appl. Phys. Lett.* **118**, 071905 (2021).
- [15] L. Zhou, F. Li, J.-X. Liu, Q. Hu, W. Bao, Y. Wu, X. Cao, F. Xu, and G.-J. Zhang, *J. Eur. Ceram. Soc.* **40**, 5731–5739 (2020).
- [16] J. Zhu, X. Meng, P. Zhang, Z. Li, J. Xu, M. J. Reece, and F. Gao, *J. Eur. Ceram. Soc.* **41**, 2861–2869 (2021).
- [17] T. J. Harrington, J. Gild, P. Sarker, C. Toher, C. M. Rost, O. F. Dippo, C. McElfresh, K. Kaufmann, E. Marin, L. Borowski, P. E. Hopkins, J. Luo, S. Curtarolo, D. W. Brenner, and K. S. Vecchio, *Acta Mater.* **166**, 271–280 (2019).
- [18] T. Csanádi, M. Vojtko, Z. Dankházi, M. J. Reece, and J. Dusza, *J. Eur. Ceram. Soc.* **40**, 4774–4782 (2020).
- [19] D. Moskovskikh, S. Vorotilo, V. Buinevich, A. Sedegov, K. Kuskov, A. Khort, C. Shuck, M. Zhukovskiy, and A. Mukasyan, *Sci. Rep.* **10**, 19874 (2020).
- [20] V. Braic, M. Balaceanu, M. Braic, A. Vladescu, S. Panseri, and A. Russo, *J. Mech. Behav. Biomed. Mater.* **10**, 197–205 (2012).
- [21] M.-H. Tsai, C.-W. Wang, C.-H. Lai, J.-W. Yeh, and J.-Y. Gan, *Appl. Phys. Lett.* **92**, 052109 (2008).
- [22] A. Sarkar, L. Velasco, D. Wang, Q. Wang, G. Talasila, L. de Biasi, C. Kübel, T. Brezesinski, S. S. Bhattacharya, H. Hahn, and B. Breitung, *Nat. Commun.* **9**, 3400 (2018).
- [23] Y. Chen, H. Fu, Y. Huang, L. Huang, X. Zheng, Y. Dai, Y. Huang, and W. Luo, *ACS Mater. Lett.* **3**, 160–170 (2021).
- [24] M. Fracchia, P. Ghigna, T. Pozzi, U. Anselmi Tamburini, V. Colombo, L. Braglia, and P. Torelli, *J. Phys. Chem. Lett.* **11**, 3589–3593 (2020).
- [25] J. L. Braun, C. M. Rost, M. Lim, A. Giri, D. H. Olson, G. N. Kotsonis, G. Stan, D. W. Brenner, J.-P. Maria, and P. E. Hopkins, *Adv. Mater.* **30**, 1805004 (2018).
- [26] Y. Zheng, M. Zou, W. Zhang, D. Yi, J. Lan, C.-W. Nan, and Y.-H. Lin, *J. Adv. Ceram.* **10**, 377–384 (2021).
- [27] B. Jiang, Y. Yu, J. Cui, X. Liu, L. Xie, J. Liao, Q. Zhang, Y. Huang, S. Ning, B. Jia, B. Zhu, S. Bai, L. Chen, S. J. Pennycook, and J. He, *Science* **371**, 830–834 (2021).
- [28] B. Jiang, Y. Yu, H. Chen, J. Cui, X. Liu, L. Xie, and J. He, *Nat. Commun.* **12**, 3234 (2021).
- [29] Y. Sharma, Q. Zheng, A. R. Mazza, E. Skoropata, T. Heitmann, Z. Gai, B. Musico, P. F. Miceli, B. C. Sales, V. Keppens, M. Brahlek, and T. Z. Ward, *Phys. Rev. Materials* **4**, 014404 (2020).
- [30] Y. Pu, Q. Zhang, R. Li, M. Chen, X. Du, and S. Zhou, *Appl. Phys. Lett.* **115**, 223901 (2019).
- [31] J. Liu, K. Ren, C. Ma, H. Du, and Y. Wang, *Ceram. Int.* **46**, 20576–20581 (2020).
- [32] M. Zhang, X. Xu, Y. Yue, M. Palma, M. J. Reece, and H. Yan, *Mater. Des.* **200**, 109447 (2021).
- [33] G. N. Kotsonis, P. B. Meisenheimer, L. Miao, J. Roth, B. Wang, P. Shafer, R. Engel-Herbert, N. Alem, J. T. Heron, C. M. Rost, and J.-P. Maria, *Phys. Rev. Materials* **4**, 100401 (2020).
- [34] M. Qin, J. Gild, H. Wang, T. Harrington, K. S. Vecchio, and J. Luo, *J. Eur. Ceram. Soc.* **40**, 4348–4353 (2020).

- [35] L. Feng, W.-T. Chen, W. G. Fahrenholtz, and G. E. Hilmas, *J. Am. Ceram. Soc.* **104**, 419–427 (2021).
- [36] A. Vojdani Saghir, S. Mollazadeh Beidokhti, J. Vahdati Khaki, and A. Salimi, *J. Eur. Ceram. Soc.* **41**, 563–579 (2021).
- [37] W. Zhang, L. Chen, C. Xu, W. Lu, Y. Wang, J. Ouyang, and Y. Zhou, *J. Mater. Sci. Technol.* **72**, 23–28 (2021).
- [38] L. Feng, W. G. Fahrenholtz, and G. E. Hilmas, *J. Am. Ceram. Soc.* **102**, 7217–7224 (2019).
- [39] T. Li, Y. Yao, Z. Huang, P. Xie, Z. Liu, M. Yang, J. Gao, K. Zeng, A. H. Brozena, G. Pastel, M. Jiao, Q. Dong, J. Dai, S. Li, H. Zong, M. Chi, J. Luo, Y. Mo, G. Wang, C. Wang, R. Shahbazian-Yassar, and L. Hu, *Nat. Catal.* **4**, 62–70 (2021).
- [40] A. Zunger, S.-H. Wei, L. G. Ferreira, and J. E. Bernard, *Phys. Rev. Lett.* **65**, 353–356 (1990).
- [41] K. Yang, C. Oses, and S. Curtarolo, *Chem. Mater.* **28**, 6484–6492 (2016).
- [42] K. Kaufmann, D. Maryanovsky, W. M. Mellor, C. Zhu, A. S. Rosengarten, T. J. Harrington, C. Oses, C. Toher, S. Curtarolo, and K. S. Vecchio, *npj Comput. Mater.* **6**, 42 (2020).
- [43] D. G. Sangiovanni, F. Tasnádi, T. Harrington, M. Odén, K. S. Vecchio, and I. A. Abrikosov, *Mater. Des.* **204**, 109634 (2021).
- [44] F.-Z. Dai, Y. Sun, B. Wen, H. Xiang, and Y. Zhou, *J. Mater. Sci. Technol.* **72**, 8–15 (2021).
- [45] D. Demirskiy, T. S. Suzuki, K. Yoshimi, and O. Vasylykiv, *Open Ceramics* **2**, 100015 (2020).
- [46] K. Lu, J.-X. Liu, X.-F. Wei, W. Bao, Y. Wu, F. Li, F. Xu, and G.-J. Zhang, *J. Eur. Ceram. Soc.* **40**, 1839–1847 (2020).
- [47] C. M. Rost, Z. Rák, D. W. Brenner, and J.-P. Maria, *J. Am. Ceram. Soc.* **100**, 2732–2738 (2017).
- [48] Z. Rák, J.-P. Maria, and D. W. Brenner, *Mater. Lett.* **217**, 300–303 (2018).
- [49] P.-K. Huang and J.-W. Yeh, *Scr. Mater.* **62**, 105–108 (2010).
- [50] F. Wang, X. Zhang, X. Yan, Y. Lu, M. Nastasi, Y. Chen, and B. Cui, *J. Am. Ceram. Soc.* **103**, 4463–4472 (2020).
- [51] B. Ye, T. Wen, K. Huang, C.-Z. Wang, and Y. Chu, *J. Am. Ceram. Soc.* **102**, 4344–4352 (2019).
- [52] Y. Wang, T. Csanádi, H. Zhang, J. Dusza, M. J. Reece, and R.-Z. Zhang, *Adv. Theory Simul.* **3**, 2000111 (2020).
- [53] P. H. Mayrhofer, A. Kirnbauer, Ph. Ertelthaler, and C. M. Koller, *Scr. Mater.* **149**, 93–97 (2018).
- [54] V. F. Gorban', A. A. Andreev, G. N. Kartmazov, A. M. Chikryzhov, M. V. Karpets, A. V. Dolomanov, A. A. Ostroverkh, and E. V. Kantsyr, *J. Superhard Mater.* **39**, 166–171 (2017).
- [55] S.-C. Liang, Z.-C. Chang, D.-C. Tsai, Y.-C. Lin, H.-S. Sung, M.-J. Deng, and F.-S. Shieu, *Appl. Surf. Sci.* **257**, 7709–7713 (2011).
- [56] O. V. Sobol', A. A. Andreev, V. F. Gorban', N. A. Krapivka, V. A. Stolbovoi, I. V. Serdyuk, and V. E. Fil'chikov, *Tech. Phys. Lett.* **38**, 616–619 (2012).
- [57] C. Peng, X. Gao, M. Wang, L. Wu, H. Tang, X. Li, Q. Zhang, Y. Ren, F. Zhang, Y. Wang, B. Zhang, B. Gao, Q. Zou, Y. Zhao, Q. Yang, D. Tian, H. Xiao, H. Gou, W. Yang, X. Bai, W. L. Mao, and H.-k. Mao, *Appl. Phys. Lett.* **114**, 011905 (2019).
- [58] D. Demirskiy, T. Nishimura, T. S. Suzuki, Y. Sakka, O. Vasylykiv, and K. Yoshimi, *J. Asian Ceram. Soc.* **8**, 1262–1270 (2020).
- [59] X. Han, V. Girman, R. Sedlak, J. Dusza, E. G. Castle, Y. Wang, M. Reece, and C. Zhang, *J. Eur. Ceram. Soc.* **40**, 2709–2715 (2020).
- [60] M. D. Hossain, T. Borman, A. Kumar, X. Chen, A. Khosravani, S. R. Kalidindi, E. A. Paisley, M. Esters, C. Oses, C. Toher, S. Curtarolo, J. M. LeBeau, D. Brenner, and J.-P. Maria, *Acta Mater.* **215**, 117051 (2021).
- [61] J.-X. Liu, X.-Q. Shen, Y. Wu, F. Li, Y. Liang, and G.-J. Zhang, *J. Adv. Ceram.* **9**, 503–510 (2020).
- [62] C. M. Rost, T. Borman, M. D. Hossain, M. Lim, K. F. Quiambao-Tomko, J. A. Tomko, D. W. Brenner, J.-P. Maria, and P. E. Hopkins, *Acta Mater.* **196**, 231–239 (2020).
- [63] D. Liu, A. Zhang, J. Jia, J. Meng, and B. Su, *J. Eur. Ceram. Soc.* **40**, 2746–2751 (2020).
- [64] A. J. Wright, Q. Wang, S.-T. Ko, K. M. Chung, R. Chen, and J. Luo, *Scr. Mater.* **181**, 76–81 (2020).
- [65] H. Chen, H. Xiang, F.-Z. Dai, J. Liu, Y. Lei, J. Zhang, and Y. Zhou, *J. Mater. Sci. Technol.* **35**, 1700–1705 (2019).
- [66] X. Yan, L. Constantin, Y. Lu, J.-F. Silvain, M. Nastasi, and B. Cui, *J. Am. Ceram. Soc.* **101**, 4486–4491 (2018).
- [67] Y. Sharma, A. R. Mazza, B. L. Musico, E. Skoropata, R. Nepal, R. Jin, A. V. Ievlev, L. Collins, Z. Gai, A. Chen, M. Brahlek, V. Keppens, and T. Z. Ward, *ACS Appl. Mater. Inter.* **13**, 17971–17977 (2021).
- [68] L. Zhou, F. Li, J.-X. Liu, S.-K. Sun, Y. Liang, and G.-J. Zhang, *J. Hazard. Mater.* **415**, 125596 (2021).
- [69] P. B. Meisenheimer, L. D. Williams, S. H. Sung, J. Gim, P. Shafer, G. N. Kotsonis, J.-P. Maria, M. Trassin, R. Hovden, E. Kioupakis, and J. T. Heron, *Phys. Rev. Materials* **3**, 104420 (2019).
- [70] V. Jacobson, D. Diercks, B. To, A. Zakutayev, and G. Brennecke, *J. Eur. Ceram. Soc.* **41**, 2617–2624 (2021).
- [71] B. Ye, T. Wen, D. Liu, and Y. Chu, *Corros. Sci.* **153**, 327–332 (2019).
- [72] B. Ye, T. Wen, and Y. Chu, *J. Am. Ceram. Soc.* **103**, 500–507 (2020).
- [73] Y. Tan, C. Chen, S. Li, X. Han, J. Xue, T. Liu, X. Zhou, and H. Zhang, *J. Alloys Compd.* **816**, 152523 (2020).
- [74] L. Backman, J. Gild, J. Luo, and E. J. Opila, *Acta Mater.* **197**, 20–27 (2020).
- [75] L. Backman, J. Gild, J. Luo, and E. J. Opila, *Acta Mater.* **197**, 81–90 (2020).
- [76] Y. Wang, R.-Z. Zhang, B. Zhang, O. Skurikhina, P. Balaz, V. Araullo-Peters, and M. J. Reece, *Corros. Sci.* **176**, 109019 (2020).
- [77] H. Wang, S. Wang, Y. Cao, W. Liu, and Y. Wang, *J. Mater. Sci. Technol.* **60**, 147–155 (2021).
- [78] H. Wang, Y. Cao, W. Liu, and Y. Wang, *Ceram. Int.* **46**, 11160–11168 (2020).
- [79] N. Qiu, H. Chen, Z. Yang, S. Sun, Y. Wang, and Y. Cui, *J. Alloys Compd.* **777**, 767–774 (2019).
- [80] D. Bérardan, S. Franger, A. K. Meena, and N. Dragoe, *J. Mater. Chem. A* **4**, 9536–9541 (2016).
- [81] E. Lökçü, C. Toparli, and M. Anik, *ACS Appl. Mater. Inter.* **12**, 23860–23866 (2020).
- [82] Z. Lun, B. Ouyang, D.-H. Kwon, Y. Ha, E. E. Foley, T.-Y. Huang, Z. Cai, H. Kim, M. Balasubramanian, Y. Sun, J. Huang, Y. Tian, H. Kim, B. D. McCloskey, W. Yang, R. J. Clément, H. Ji, and G. Ceder, *Nat. Mater.* **20**, 214–221 (2021).
- [83] J. Wang, Y. Cui, Q. Wang, K. Wang, X. Huang, D. Stenzel, A. Sarkar, R. Amzi, T. Bergfeldt, S. S. Bhattacharya,

- R. Kruk, H. Hahn, S. Schweidler, T. Brezesinski, and B. Breitung, *Sci. Rep.* **10**, 18430 (2020).
- [84] F. Tavani, M. Fracchia, N. Pianta, P. Ghigna, E. Quartarone, and P. D'Angelo, *Chem. Phys. Lett.* **760**, 137968 (2020).
- [85] P. Ghigna, L. Airoidi, M. Fracchia, D. Callegari, U. Anselmi-Tamburini, P. D'Angelo, N. Pianta, R. Ruffo, G. Cibin, D. O. de Souza, and E. Quartarone, *ACS Appl. Mater. Int.* **12**, 50344–50354 (2020).
- [86] T. X. Nguyen, Y.-H. Su, C.-C. Lin, J. Ruan, and J.-M. Ting, *Adv. Sci.* **8**, 2002446 (2021).
- [87] Y. Gao, Y. Mao, Z. Song, X. Zhao, J. Sun, W. Wang, G. Chen, and S. Chen, *Appl. Energy.* **279**, 115777 (2020).
- [88] H. Xu, Z. Zhang, J. Liu, C.-L. Do-Thanh, H. Chen, S. Xu, Q. Lin, Y. Jiao, J. Wang, Y. Wang, Y. Chen, and S. Dai, *Nat. Commun.* **11**, 3908 (2020).
- [89] S. Zhai, J. Rojas, N. Ahlborg, K. Lim, M. F. Toney, H. Jin, W. C. Chueh, and A. Majumdar, *Energy Environ. Sci.* **11**, 2172–2178 (2018).
- [90] Y. Wei, M. Zhang, P. Wu, J. Luo, D. Tao, C. Peng, L. Dai, L. Wang, H. Li, and W. Zhu, *Appl. Surf. Sci.* **529**, 146980 (2020).
- [91] F. Wang, X. Yan, T. Wang, Y. Wu, L. Shao, M. Nastasi, Y. Lu, and B. Cui, *Acta Mater.* **195**, 739–749 (2020).